ROYAL SOCIETY
OF CHEMISTRY

PAPER

Check for updates

Fluorine-free nanoparticle coatings on cotton fabric: comparing the UV-protective and hydrophobic capabilities of silica *vs.* silica-ZnO nanostructures

Irene ChaoYun Liu, Xin Hu, Bin Fei, Chenghao Lee, Suju Fan, John H. Xin and Nuruzzaman Noor [ID] *

Robust, hydrophobic woven cotton fabrics were obtained through the sol–gel dip coating of two different nanoparticle (NP) architectures; silica and silica-ZnO. Water repellency values as high as 148° and relatively low tilt angles for fibrous fabrics (12°) were observed, without the need for fluorinated components. In all cases, this enhanced functionality was achieved with the broad retention of water vapor permeability characteristics, *i.e.*, less than 10% decrease. NP formation routes indicated direct bonding interactions in both the silica and silica-ZnO structures. The physico-chemical effects of NP-compatibilizer (*i.e.*, polydimethoxysilane (PDMS) and *n*-octyltriethoxysilane (OTES) at different ratios) coatings on cotton fibres indicate that compatibilizer-NP interactions are predominantly physical. Whenever photoactive ZnO-containing additives were used, there was a minor decrease in hydrophobic character, but order of magnitude increases in UV-protective capability (*i.e.*, UPF > 384); properties which were absent in non-ZnO-containing samples. Such water repellency and UPF capabilities were stable to both laundering and UV-exposure, resisting the commonly encountered UV-induced wettability transitions associated with photoactive ZnO. These results suggest that ZnO-containing silica NP coatings on cotton can confer both excellent and persistent surface hydrophobicity as well as UV-protective capability, with potential uses in wearables and functional textiles applications.

1. Introduction

Surface functionalization of textiles for hydrophobic (*i.e.*, water-repellent) and ultraviolet (UV)-protective capability is increasingly important for high-performance technical textiles, outdoor wear and protective fabrics applications.[1,2] Cellulosic cotton is the most widely used natural fibre in the textile industry and comprises numerous surface hydroxyl groups, which renders such substrates intrinsically hydrophilic and hygroscopic.[3–5] Thus, effective, durable and stable functionalization routes for controlling cotton wettability are of great interest.

Organosilicon and fluoropolymer-based compounds are reliably used to fabricate superhydrophobic textile surfaces while also keeping fabrics relatively soft and breathable.[6,7] Perfluorinated compounds (PFC), depending on their structure, can yield highly water-repellent surfaces due to their ability to lower surface energy below that of any other common chemical treatment.[8] However, PFC are often expensive, environmentally persistent – over a decade in some cases – and pose potential

human-health issues, *e.g.*, can interfere with reproductive and endocrine systems as well as stimulate tumor growth.[9,10] Therefore, fluorine-free, low cost and environment-benign hydrophobic technologies are in favor.[11,12] Silica-based, and zinc oxide (ZnO)-based coatings are popular alternatives.

Surface wetting is determined by static contact angle measurements; hydrophobic surfaces exhibit a contact angle between a droplet and surface exceeding 90° (superhydrophobic when above 150°), which often also results in a low sliding angle, below 10°, although this is often higher for fibrous substrates with complex, irregular microstructures.[13,14] Conference of surface (super-)hydrophobicity usually requires: (i) modification for a low surface energy and; (ii) a hierarchical nano/micron-scale topographical roughness (to minimize contact areas between a liquid droplet and the solid surface).[15,16] Both conditions, as well as any electrostatic interactions, decrease the sliding resistance and so, tilt angle of an impingent water droplet, based on differing liquid–solid lateral adhesion forces in both the static and kinetic regimes, reflecting improved water repellency.[17,18]

Silica-based coatings fulfil the first requirement of surface hydrophobicity, while offering low environmental and bio-accumulation risks, as well as being durable; resistant to

The Hong Kong Polytechnic University, School of Fashion and Textiles, Materials Synthesis and Processing Lab, Hung Hom, Kowloon, Hong Kong SAR. E-mail: nzmnoor@outlook.com

mechanical abrasion, and stable to liquids exposure.[19,20] However, inorganic PFC-alternatives best satisfy the second hydrophobic condition, and also possess excellent robustness, *e.g.*, photoactive ZnO nanoparticles (NP) present surface-roughened hydrophobicity and can also absorb UV-radiation – beneficial properties that silica alone cannot provide.[21–23] Such ZnO UV-shielding capabilities have been used both in cosmetics and wearables.[24,25] Fabric UV-blocking is characterized by the UV protective factor (UPF), which protects against both UV-A (320–400 nm) and UV-B (280–320 nm) radiation sources to *e.g.*, erythema, among other issues.[26,27] Such optically-protective coatings help surfaces resist UV-photodegradation, *e.g.*, reduced photo-yellowing of wool.[28,29] However, an issue with ZnO (and other photoactive metal oxides) is that UV-exposure, even briefly, often causes a light-induced transition, *e.g.*, UV-induced superhydrophilicity; transforming from super-hydrophobic to superhydrophilic, or *vice versa*.[30,31] Nano-composite structures that resist such transitions would allow for reliably consistent functional properties over time – a critical requirement for many commercial applications.

The objective of this work was to compare silica NP and silica-ZnO NP coated substrate effects, and show that ZnO presence affords dual UV-protective and water-repellency properties, while also being resistant to UV-induced changes in surface wettability. Although similar architectures have been reported for drug delivery, bio-imaging, photonics and other applications, such combined silica-ZnO structures are less well-explored for textile functionalization.[32–34] Both structures are also fluorine-free, relatively benign in nature, have proven capability, are cost-efficient, and separately, are already ubiquitous in wearables applications.[35]

Silane-type coupling agents act as interfacial adhesives between an inorganic material and organic substrates, *e.g.*, in textiles, enhancing loading, dispersion and binding.[36,37] Poly(dimethyl-siloxane) (PDMS) and *n*-octyltriethoxysilane (OTES) – two commonly used long-chain alkoxide hydrophob-izing agents – were used at different loadings in this study to help graft the NP to substrates and so, enhance the overall hydrophobic surface properties.[38–40] Absent the use of such agents, the durability of NP coatings on textiles is greatly diminished. We identified which compatibilizer was most effective for hydrophobic and UPF applications respectively.

A directly-controllable sol–gel dip coating approach was used on fabrics to impart roughness and increase hydrophobicity, *via* loading of pre-formed NP. This deposition method does not need salt, electrolytes, or extended high-temperature process-ing, unlike other common coating techniques.[41–43] The resultant composites were observed for differences in hydrophobicity and UPF functionality, as well as the relative stability of such fabric coatings to UV-light exposure and extended laundering treatments.

2. Methodology

2.1 Chemicals

Chemicals used as-received were; acetone (VWR); ammonia, (VWR, 28–32%); ethanol absolute (EtOH, Unichem, 99.5%); *n*-octyltriethoxysilane (OTES, Alfa Aesar, 95%); poly(dimethyl-siloxane) (PDMS, Sigma Aldrich, M_w = 95 000); sodium hydroxide (NaOH, International Laboratory, USA); tetraethylor-thosilicate (TEOS, $(Si(OC_2H_5)_4)$, Sigma-Aldrich, 98%); toluene (VWR-Chem AR); triethanolamine (TEA, Xiliong Chemical, 98%); zinc acetate dihydrate ($Zn(OAc)_2$, Acros Organic) and deionized (DI) water (18 MΩ).

2.2 Substrate

Woven, bleached, pre-washed cotton fabric substrates of 1 × 1 inch (2.54 × 2.54 cm × ∼0.2 mm; l × w × t) were used for deposition. To remove any impurities, substrates were cleaned with a non-ionic aqueous detergent mixture in a washing machine at 85 °C for 15 min, then rinsed with DI water.

2.3 Two-step synthesis

(1) Preparation of silica and silica-ZnO NP: silica NP were prepared *via* the Stöber method comprising hydrolysis then subsequent, or even concurrent, condensation.[44,45] TEOS (25 ml; silica precursor), water (75 ml) and $NH_3·H_2O$ (25 ml; catalyst) were mixed under stirring, then aged for 4 h.[46] Products were collected by centrifu-gation and washed three times with ethanol, then oven-dried. To prepare silica-ZnO composites, a simplified controlled chemical double jet precipitation technique was used by adding TEA precipitating agent and $Zn(OAc)_2$ precursor into a silica-ethanol aqueous solution simultaneously.[47,48] Briefly, silica (0.2 g) was dispersed in a 30 mL EtOH–water solution and the mixture heated to 90 °C. After 10 min, 10 ml of 1.6 mol L^{-1} TEA and 20 ml of 0.02 mol L^{-1} $Zn(OAc)_2$ solution were dropped simultaneously into the silica-EtOH aqueous solution at a constant flow rate. The system was then stirred continuously at 90 °C for 1 h. The resulting white powders were centrifuged, washed repeatedly with distilled water, and oven-dried. Finally, the powders were sintered for 3 h at 700 °C to remove the TEA, resulting in the silica-ZnO NP material. Such formation routes yield Si–O–Si bonding structures, as well as points of attachment that survive hydrolysis and condensation. (2) Coating NP onto cotton fabric substrates. Substrates were treated with the solution containing PDMS, OTES and the NP solution. First, PDMS (1.9 g) was dissolved in toluene (48 mL) and stirred for 1 h at room temperature. Then, the weight percentage concentration of 2% or 86% of OTES (relative to PDMS) was added with a further 3 h stirring at room temperature. After this, the pre-prepared NP powder (0.1 g) was ultrasonically dispersed in solution for 30 min. Subsequently, the cotton fabric was dip-coated in this mixture; a 20 min immersion period fol-lowed by withdrawal (1 cm s^{-1}), followed by a short evaporation, and then curing at 140 °C for 1 h to aid solvent removal, and allow for full densification of the oxide matrix.

2.4 UV-exposure testing

An artificial light source, UV lamp (Philips, 18 W) emitting a gauss shaped spectrum that peaked at 370 nm and with cut off at 340 nm and 400 nm respectively was used. Samples were placed under the UV lamp at a substrate-lamp distance of 16 cm, for up to 40 h.

2.5 Characterization

Nanoparticle formation was probed *via* time-resolved *in situ* analysis of reaction progress. This allowed for empirical determination of reaction mechanisms. In such cases, the desired chemicals were mixed at known ratios immediately prior to loading onto sample stages for analysis, and data acquisition done while time elapsed was recorded.[49] The morphologies and microstructures of pre-formed NP and fabric-coated samples were examined using a TESCAN VEGA3 tungsten thermionic emission scanning electron microscope (SEM) on gold sputter coated samples. Energy dispersive X-ray analysis (EDS) was also carried out along with SEM. Transmission electron microscopy (TEM) images were acquired on a JEOL JEM-2100F, inclusive of EDS elemental mapping, on gold-sputtered samples. X-ray diffraction (XRD) was used for determining crystallinity and phase purity on a Rigaku SmartLab, operated at 40 kV and 100 mA with Cu-Kα radiation in a Bragg–Brentano configuration and 5° divergence, acquired over the 15–90° 2θ range, at a 0.02° step size. UV-visible spectra of pre-formed NP mixtures were acquired on a Hitachi Double Beam Spectrophotometer UH5300, against a DI H$_2$O standard over a 250–750 nm range. Analysis of pre-formed NP mixtures using dynamic light scattering (DLS) technique was conduct on a Zetasizer nano-ZS (Malvern Panalytical, Malvern, UK) with a backscattering detection angle of 173° and a thermostat with 60 s thermal equilibration time.[50] The NP were randomly dispersed in DI-H$_2$O to determine the hydrodynamic diameters; solutions were injected into the sample cuvette that was rinsed with Milli-Q water twice and dried before use. Temperatures were maintained at room temperature during the analysis. The hydrodynamic diameter (z-average in nm) was determined from the translational diffusion coefficient, using the Stokes–Einstein equation. All measurements were taken three times and averaged.

Coated fabrics were analyzed using transmission ATR-FTIR on a PerkinElmer Spectrum 100 over 4000–650 cm^{-1} at 4 cm^{-1} resolution and 8 scans. Color strength, K/S data, was acquired on a Macbeth ColorEye (CE-7000A) colorimeter, based on D65 illuminant and 10° observer values, with a small aperture view, across 400–700 nm, with the UV filtered and the specular component excluded, across four measurements for each sample to help minimize fibre orientation effects. A SCA 20, Data-Physics Instrument video optical contact angle goniometer was used to measure surface wettability of cotton substrates, with a 15 µL DI water droplet size for all samples delivered from a needle connected to a syringe pump, at 24 $\pm$ 0.5 °C and relative humidity of 40 $\pm$ 3%.[51,52] Liquid droplets were placed onto the sample surface and the lateral, static water contact angles (WCA) measured; data continuously acquired for a 20 s period after initial impingement. All WCA were determined by averaging values measured at multiple different points on repeat sample surfaces with a water droplet of 15 µL. Because the protruding fibers have some elasticity and can thus exhibit forces on the water droplet, accurate values for advancing and receding WCA are hard to acquire, so only static WCA are reported. For sliding angle investigation *via* a tilted drop method, a drop of water was placed on the sample surface then tilted at a known angle (at step sizes of 0.5°) and the point at which the liquid droplet begins to "roll" was recorded as the sliding angle. A lower sliding angle indicates greater ease of droplet movement across and down the fabric surface.

Water vapor permeability testing was done using a modified BS7209 method. After fabrics were placed in a conditioning room overnight (at 40 $\pm$ 2 °C and 90% $\pm$ 5% RH), test samples were sealed over an open receptacle containing a known volume of water, and the assembly was placed in a controlled atmosphere at room temperature. After a 6 h pause to establish an equilibrium of water vapor pressure gradient across the sample, successive weightings of the fabric-covered assembly were made at set intervals, and the water vapor transmission rate (WVTR) was calculated to investigate the water vapor permeability using the following equation:

$$\text{WVTR} = 24M/At \tag{1}$$

where M is the mass loss of the assembly over the period of time, t (in g) is the time between successive weightings of the assembly (in h) and A is the test area of the exposed test fabric, equal to the internal area of the receptacle cups (m^2). The units are gm^{-2} 24 h.[53] WVTR is the industry standard for evaluation of water vapor permeability (*i.e.*, the capacity of substrates to resist moisture transmission through the fabric and out into the atmosphere) and is the focus of most investigations into waterproof breathable textiles. Lower values indicate higher moisture resistance, and trapped moisture which in turn causes wearer discomfort. Perspiration and evaporation allow the human body to cool down with a high WVTR and so, even waterproof fabrics must maintain a high level of breathability to ensure comfort.[53,54]

UV-visible absorbance data was acquired on a Varian Cary 300 Conc UV-vis spectrophotometer, over a 200–800 nm range at a step size of 0.5 nm. The UPF values were calculated from:

$$\text{UPF} = \frac{\sum_{290}^{400} E(\lambda) \times S(\lambda)}{\sum_{290}^{400} E(\lambda) \times S(\lambda) \times T(\lambda)} \times 100 \tag{2}$$

where $E(\lambda)$ is the CIE reference erythema dose spectrum, $S(\lambda)$ is the radiation intensity distribution of sunlight, and $T(\lambda)$ is the diffuse transmittance spectrum (%).[55,56]

2.6 Fastness to domestic and commercial laundering test

Laundering (including washing, rinsing and drying of fabrics) commonly causes coated material loss. Thus, laundering durability testing replicates the various temperature, detergent alkalinity, bleaching and friction/grinding forces encountered during a standard wash cycle. Each accelerated wash cycle is equivalent to three standard real-world, domestic wash cycles. Wash durability was evaluated at 40 °C with the equivalent of 4 g/500 ml ECE Phosphate Reference Detergent (SDC Type 3) in water, for 30 min, with ten steel balls (each weighing ~0.9 g, with a diameter of ~0.7 mm), in a Launder-O-meter (Atlas, USA).

Subsequently, all fabrics were cleaned at 40 °C with 100 ml water for each sample, for 1 min. Three accelerated wash cycles were carried out on samples, (*i.e.*, equivalent to nine standard wash cycles), after which UPF and water repellency properties were retested.

3. Results

3.1 Reaction schemes and nanoparticle analysis

Sol–gel derived silica NP and silica-ZnO NP were used to fabricate water-repellent surfaces. The formation processes of NP were analyzed (prior to their coating onto substrates), in order to understand the reaction routes (Fig. 1a–d).[49] Stöber-based silica NP were made *via* an ammonia-catalyzed, hydrolysis-condensation polymerization.[57] Simply, TEOS reacts with hydroxide to form a silanol, which condenses to the formation of siloxide ions and water. A siloxane linkage subsequently forms through attack on the silanol silicon centre (the rate-

determining step), rendering a silane network on the NP surface.[58,59] The final FTIR spectra also indicates peaks spanning 1400–1200 cm^{-1} which signal Si–O–Si bridging bonds *via* condensation; specifically, the Si–O–Si asymmetric stretch and the strained siloxane networks in amorphous silica.[60] The sharp peak around 1066 cm^{-1} represent the oxygen asymmetric stretch which is obvious in both NPs FTIR spectra.[61] This is further confirmed by the appearance of a shoulder at 946 cm^{-1} (and a weak signal at ~890 cm^{-1}) upon heat treatment.

ZnO addition was done *via* a double jet precipitation method under aqeuous, basic conditions, with initial formation of β-Zn(OH)$_2$, followed by rapid transformation to ZnO – the ethanolic conditions allowing for smaller, well-dispersed NP sizes.[62] Zn(OAc)$_2$ is decomposed into interstices of the inorganic silica network, resulting in Si–O–Zn and Si–O–Si bands, corresponding to a strong bonding interaction between ZnO and the silylating agent.[63] The FTIR peak near 1390 cm^{-1} may represent a bond between the –OH groups of the ZnO surface and TEOS
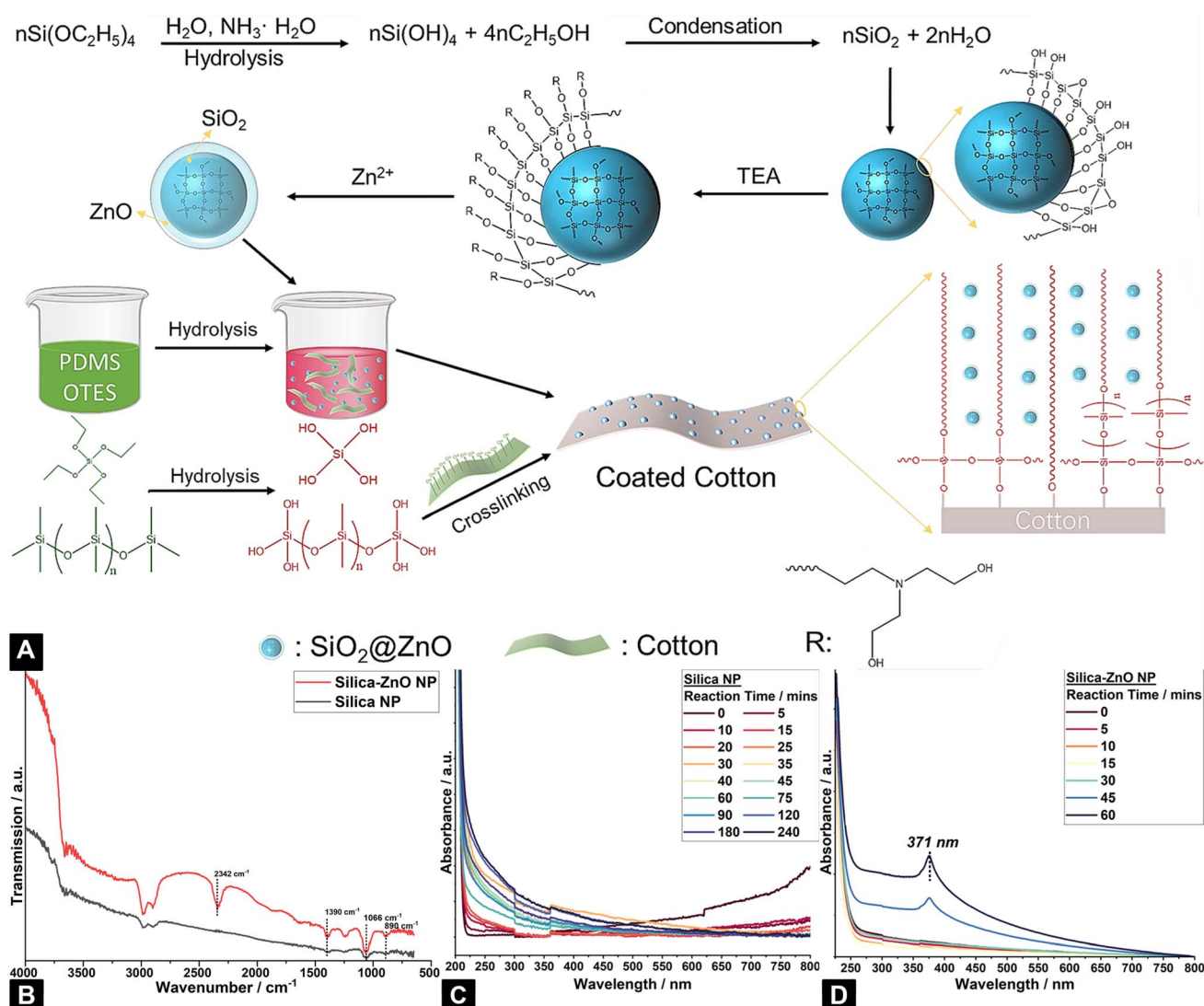

Fig. 1 (A) Reaction scheme for the nanoparticle formation and cotton fabric coating; (B) ATR-FTIR spectra of dried silica NP and silica-ZnO NP powder and, the time-resolved UV-vis analyses of silica NP (C) and silica-ZnO NP (D) formation.

carbonyl groups.[64] During this process, the silanol groups in siloxane oligomers may also react with TEA to subsequently aid further reactivity with $Zn(OAc)_2$ to form ZnO molecular clusters that can readily attach to the silica surface.[65] An obvious peak at ~ 2342 cm^{-1} in the silica-ZnO spectrum may correlate with trapped CO_2 in the air ambient.[66]

Both NP size and distribution impact the agglomeration behavior of precursor mixtures and pre-formed materials, which in turn affects hydrophobic character. UV-vis analyses of the silica-ZnO NP mixtures yield a very weak SPR-based signal with a maximum at ~ 371 nm.[67,68] This is due to the ZnO band edge absorption peak.[69,70] No detectable signals were observed for the silica NP mixtures.

Preformed NP powders were also analyzed *via* XRD (Fig. 2a). For silica NP, the peak centred at $2\theta \sim 24°$ indicates a broadly amorphous structure, although calcination seems to have resulted in partial densification, agglomeration and a tendency towards crystallinity.[71] Conversely, silica-ZnO samples show peaks characteristic of hexagonal wurtzite ZnO, indicating a *c*-axis preferential orientation along the (002) direction, which corresponds well with the TEM data, and is often reported with low-temperature ZnO synthesis routes.[72] There is also a slight amorphous background signal between 21 and 24° that can be

attributed to silica presence. No other phases or impurities were detected. From DLS (Fig. 2b), the silica-ZnO and silica NP mean hydrodynamic radii were ~ 145 nm and ~ 225 nm (with particle count frequency ranges of 130–150 nm and 160–240 nm), respectively. Also, single, narrow distribution curves were observed for both sample types, which indicates well-dispersed, uniform particle sizes without various aggregates. Both types of NP seemingly have relatively similar size distributions, with the silica-ZnO samples marginally smaller – the ZnO potentially inhibited agglomeration and Ostwald ripening of silica, while the effects of variant synthesis conditions also undoubtedly affect the reaction process, to impact particle size and distribution.[73–75]

TEM images of the pre-formed silica NP and silica-ZnO NP, along with their elemental analyses – measured across the respective particle clusters diameters *via* an EDS line scan function[76] – are shown in Fig. 2c and d. All samples display well-defined particles and related aggregates, with an acceptable dispersion for TEM observation. The mean silica particle size was ~ 420 nm; the larger sizes as compared to DLS measurement perhaps a result of small particle agglomerates. The surface morphology of the silica matrix was atomically rough implying uneven thickness and no discernible lattice fringes
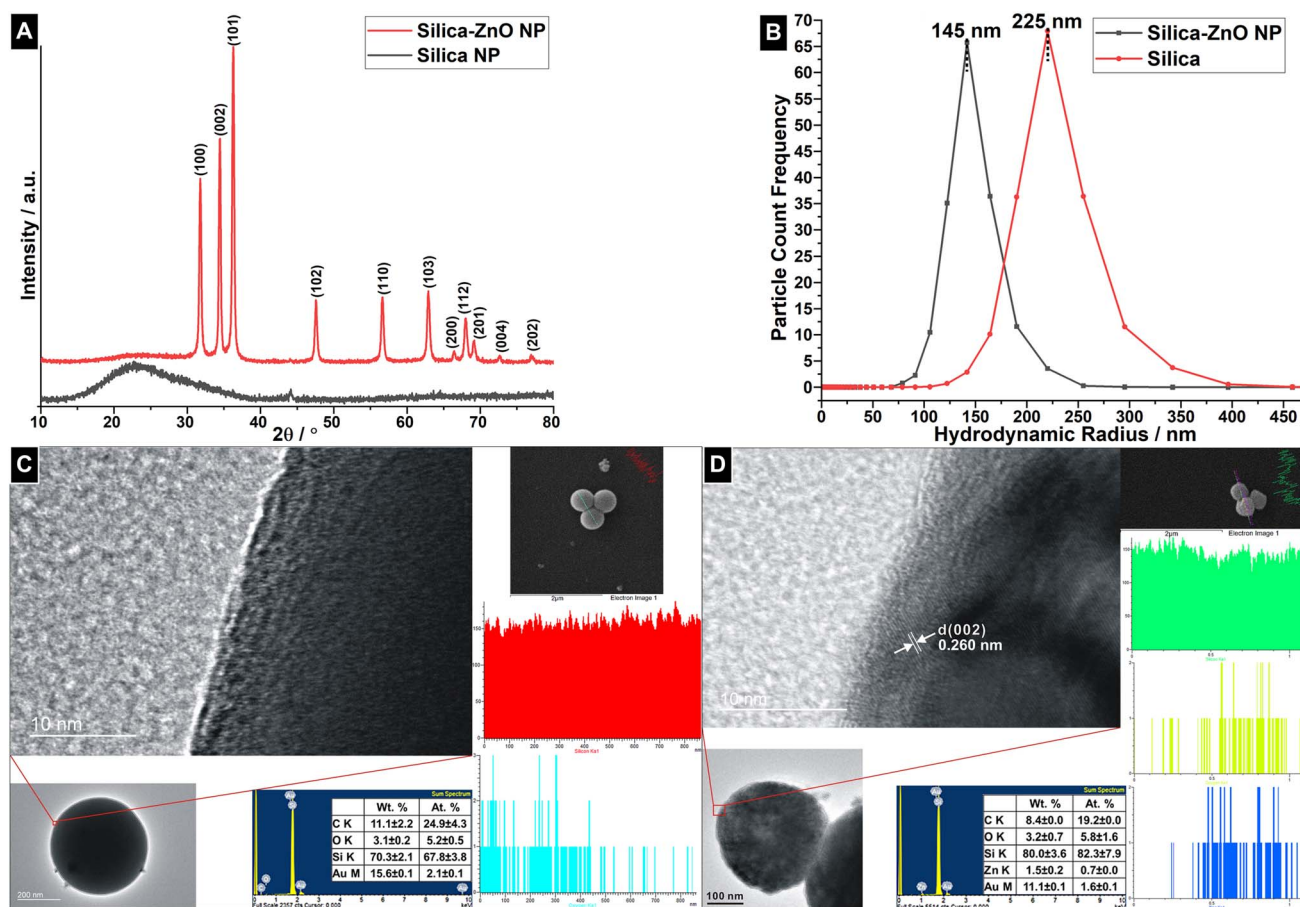

Fig. 2 (A) XRD analyzes of silica NP and silica–ZnO NP powders; (B) DLS comparison of silica NP and silica–ZnO NP mixtures, and; TEM and elemental line scan analyses (with averaged area scan elemental composition tables inset) of; (C) pre-formed silica NP powder and; (D) pre-formed silica–ZnO NP powder.

were observed, indicating that no inclusions were embedded (*e.g.*, no ZnO lattice structures). Conversely, dark lattice spacing stripes were observed in silica-ZnO NP at 10 nm scale, with *d*-spacings of 2.60 Å solely discernible, consistent with the standard ZnO (002) crystalline plane of a hexagonal structure.[77,78] Elemental compositions indicate the sole presence of silica in the silica NP, with broad spectrum presence throughout the entire NP diameter.[79] Conversely, the silica-ZnO NP clearly exhibit Zn-Mα element presence (usually concurrent with the O-Kα signal), albeit at low concentrations and without any clear maxima or minima in the distribution observable.[80]

3.2 Coated fabric characterization and testing

Sol–gel dip coatings of the NP formulations were made using two hydrophobizing agents, *i.e.*, PDMS and OTES. These intrinsically water-repellent silicone thermoset polymers undergo covalent cross-linking to the fabric surface during curing, forming a rigid network of polymer chains that potentially stabilizes NP additives onto the woven cotton substrates; the microporous matrix seemingly stabilizing high particle dispersions.[81,82] Two different ratios of PDMS : OTES were used (*i.e.*, OTES at 2% and 86% loading by weight respectively), in order to observe the different effects of such binder/hydrophobizing agent towards hydrophobic properties as well as NP loading. This difference arises because PDMS terminates in trimethylsilyl groups whereas OTES contains non-polar C–C(H) groups; the latter should allow for higher NP-additive loading due to enhanced covalent cross-linking, potentially leading to additive-derived effects.[83,84] For the NP additives, the solvated zinc acetate precursor may initially bridge between the silica and PDMS, which, after heat treatment and/or extended UV exposure, the –O group from resultant tetrahedral ZnO forms hydrogen bonds with the –H group of PDMS (*i.e.*, Si–O–Zn linkages), enhancing the overall adhesion properties.[85,86] Alternatively, in the absence of such binding effects, the ZnO NP may form embedded nanostructures.[87]

Coated fabrics were used without further modification and exhibited non-wetting behavior for water, to different degrees, absent the need for fluorine-containing agents.[88] This is in stark contrast to the cotton reference which is intrinsically absorptive, and offers no discernible wettability data. The generally colorless NP afforded little color change to the substrates, aided by the sparseness of coating and low loadings used.[89] Coatings showed good adhesion to substrates, the resulting surfaces were stable to repeated wetting, rubbing and bending.

Fabric coated samples had no clearly discernible FTIR peaks, only a muting of the cellulose signals which increases with higher silica loading (Fig. 3a).[90,91] This indicates that incorporation and interaction between the NP and compatibilizers is predominantly a physical (not chemical) one. The CIE $L^*a^*b^*$ color scale allows for tonal variations between samples to be identified (Fig. 3b and c). When compared to the reference cotton standard, L^*, (a more positive value indicating a lighter sample), shows a minor drop for all samples. The a^* values (more positive for a greater red contribution; a more negative for increasing green), show a positive increment with increased

material loading, with the highest value for NP inclusions. The b^* values (more positive for a greater yellow contribution; a more negative for increasing blue) are generally positive and similar for all except silica NP. Any addition to the substrate increases the color strength, K/S; the NP structures causing the greatest increase, although seemingly to similar extents, which is reasonable since both are composed of absorbing materials – the silica NP being marginally higher than the silica-ZnO. This is also expected due to the milky instead of pure white color shade of silica NP powders.[92]

Since hydrophobicity and its variation depends at least partly, on surface roughness, imaging was done on coated substrates to determine morphology. SEM images of the silica-based materials indicate clear presence of well-distributed, discontinuous coatings as surface irregularities due to particle clusters on cotton fibres (Fig. 3d). In all cases, a classical spherical-type structure is observed, of relatively uniform size ($\sim$0.5–2 μm), with little variation in morphology of granular protrusions between the different coating arrangements. Moreover, measurements seemingly correspond well to both particle size and TEM analyses. Further, fabric elemental analysis *via* EDS seems to corroborate the hypothesis that a higher relative amount of OTES results in a greater loading of material; there is significantly more zinc detected when more OTES was used.

From the static WCA as a function of time (Fig. 4a and b), all coated samples displayed hydrophobicity, as compared to an uncoated cotton fabric reference. On fibrous hydrophobic surfaces, water forms bead-like drops in order to reduce surface free energy, and this was especially the case for the NP-containing samples; WCA values reliably far in excess of the solely PDMS-OTES coating indicate that repellency enhancements are mainly due to NP addition, and are not predominantly silicone binder material based.[93,94] However, both sample conditions containing higher OTES (86%) presented an overall better hydrophobic character due to the hydrophobic nature of the OTES 8-carbon hydrocarbon chain.[95] With only the siliceous hydrophobizing agents, the lowest WCA values and the shortest latency periods before droplet diffusion through the substrate, was discovered for OTES(2%)-PDMS samples, in association with the highest obtained sliding angle of 19°.

Although certain individual samples showed superhydrophobic character (*i.e.*, water contact angle as high as 169° for OTES(2%)-PDMS silica-ZnO, albeit with the largest performance range), sample repeats averaged out to a reliably high hydrophobic. The most significant average WCA values were acquired from OTES(86%)-PDMS silica NP. Thus, cotton fabric was hydrophilic, PDMS-OTES coupling agents decreased the surface energy of the cotton fabric seemingly to improve hydrophobic characteristics, although this is not a long-lasting effect; impingent droplets readily pass through the porous substrate upon extended contact. Both NP structure additives created a rough surface that further increased the water repellency – slightly more so in the case of silica – to enhance the, likely Cassie-Baxter-type behavior (*i.e.*, the liquid makes partial contact balancing on the elevated regions of the solid, while also resting partly upon air pockets).[96] Moreover, the NP additives seem to stabilize fabrics to water penetration over time
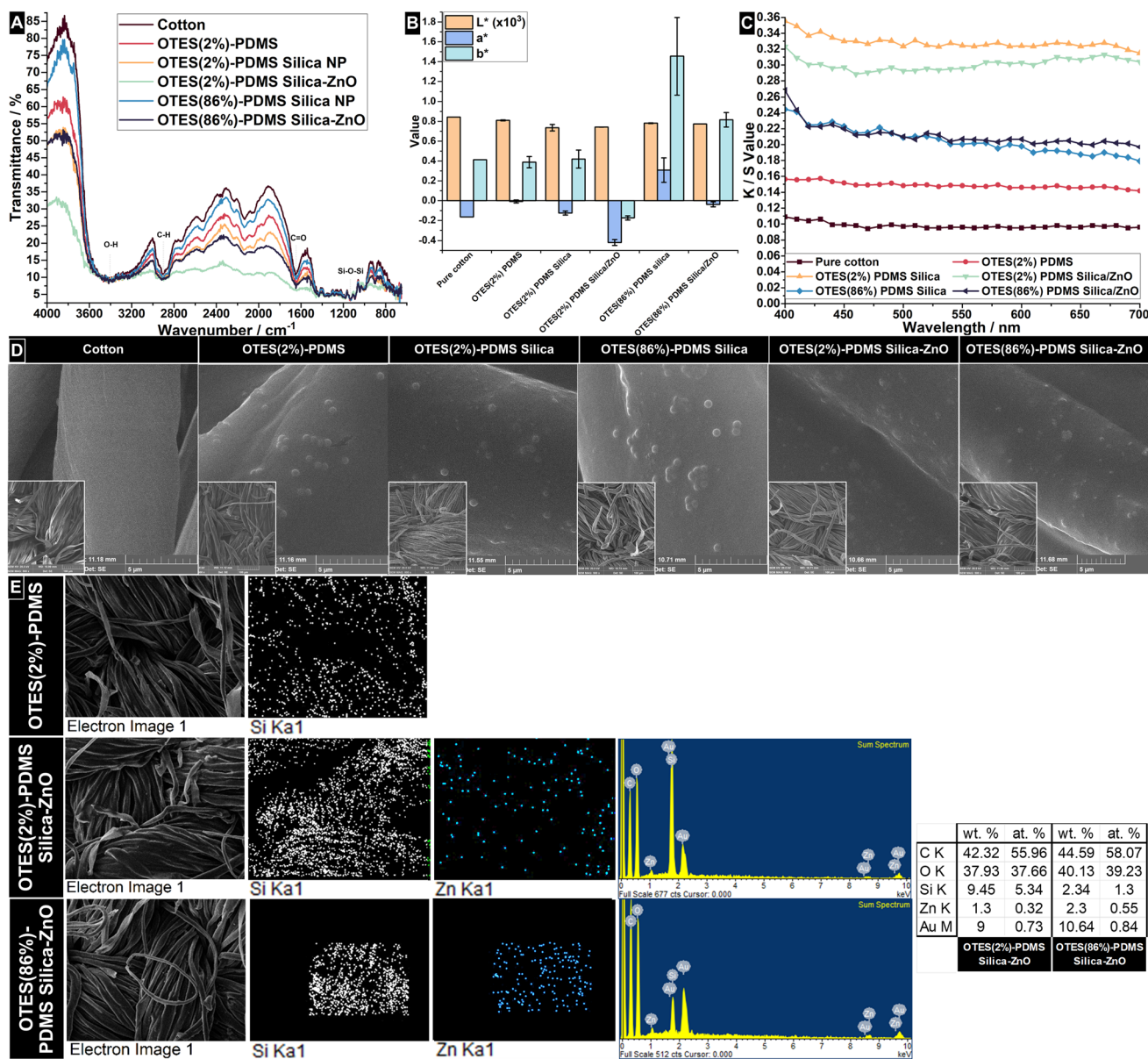
Fig. 3 (A) FTIR transmittance spectra; (B) $L*a*b*$ values; (C) K/S spectra; (D) top-down SEM images (scale 5 μm main image; scale 100 μm inset), of coated cotton substrates, and; (E) EDS elemental analyses of coated fabric substrates comparing Zn-loading.

and increased the persistence in hydrophobicity, *i.e.*, stable WCA values over 20 s; a critical factor for water-repellent wearables. The variant data between silica and ZnO NP may be explained by the different mechanisms of interaction between the different NP; the less effectively hydrophobic ZnO being more present with OTES results in lower water-repellency values.

NP-addition also afforded the greatest improvements in roll-off; the lowest sliding angle was achieved with silica-ZnO (12°), indicating improved mobility of water droplets on the surface. The varied topography caused by the two different NP coating types on the fabric surface may be related to the changes in WCA although the rough, fibrous structure of textile-based surfaces may intrinsically increase the sliding angle.[97] The NP seemingly serve to decrease the tilt angle although no sample reaches the threshold ideal of <10°.

UV-induced superhydrophilicity is a long-reported phenomenon; short bouts of UV-irradiation on surfaces containing, *e.g.*, photoactive ZnO, allowing for remarkable changes of existing surface wettability properties (*e.g.*, superhydrophilic to superhydrophobic, or *vice versa*).[98] However, in this study, whenever ZnO was used, no meaningful changes in wettability were observed, *i.e.*, even after 40 h of 370 nm UV light exposure, which suggests that silica-ZnO combinations broadly stabilize ZnO to light-induced changes – an extremely valuable steadying mechanism for reliable and consistent performance of coatings over an extended period.[99–101] While UV-curing of the PDMS and/or OTES may be a contributory factor, the fact that marked improvements were not seen in samples absent NP addition indicates that it has a minor effect.[102,103]
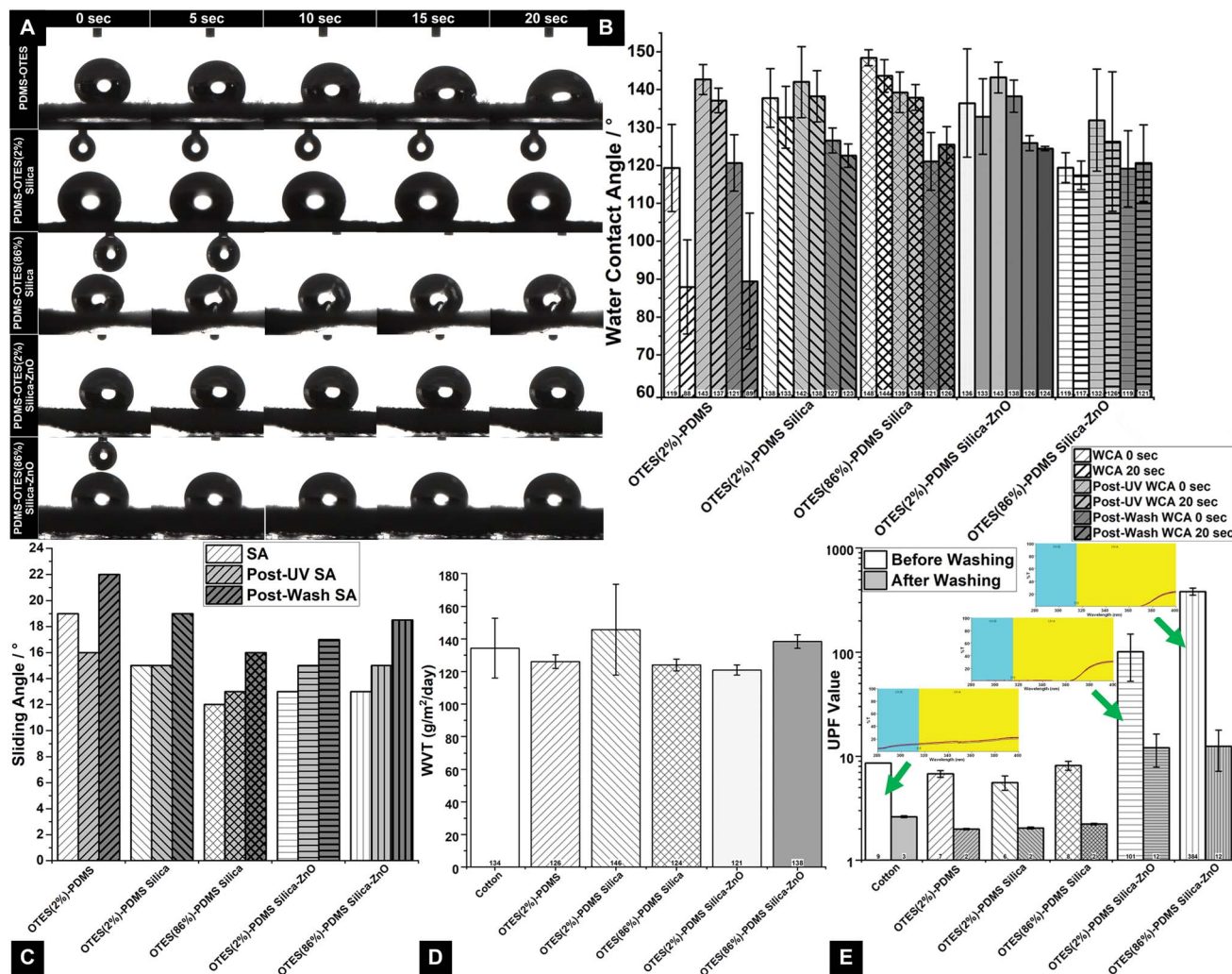
Fig. 4 Coated fabric substrate comparisons; (A) illustrative water contact angles (WCA) of the relative persistence of repellency over time for as-prepared samples; (B) average WCA for; as-obtained samples; after 40 h exposure to 370 nm, or; 3 accelerated laundering cycles; (C) sliding angle values for; as-obtained samples; after 40 h exposure to 370 nm, or; 3 accelerated laundering cycles; (D) water vapor transmission rate values of as-obtained samples, and; (E) fabric UV-protective factor pre- and post-laundering (illustrative ultraviolet-visible experimental transmittance spectra of as-prepared samples, inset).

The WVTR analyzes how much vapor passes through a material for a given size, under constant temperature and humidity conditions. Coated fabrics retained similar water vapor permeability properties, with minor decreases of ~8%, as compared to the uncoated cotton fabric references (Fig. 4d), which are acceptable for real-world usage. Thus, the hydrophobizing agent and the NP coatings had minimal effects on cotton fabric pore blockage, likely due to the relatively sparse, discontinuous coatings that result from the single-coating approach adopted, which is ideal for thermal comfort in wearables applications.[53,104] In cases where the treated sample's performance is seemingly superior to the pure cotton fabric, this is seen as an experimental variation effect. Thus, the great enhancements in both water repellence and UV protection were gained without any significant change in water vapor permeability. An extremely positive outcome.

UPF values for pure cotton and treated fabrics show that addition of silica-ZnO NP has offers at least a one order of magnitude improvement on UV-blocking capability, but only where ZnO is present (Fig. 4e).[105] This includes near-complete suppression of UV light transmission through the coated substrates across 280–370 nm (i.e., all of UV-B and much of the UV-A) – the higher the ZnO loading, the better the UV-shielding improvement. A higher amount of OTES usage also seems to allow for greater ZnO inclusion, due to its superior grafting capability as compared to PDMS.[106] Samples were also found to be UV-irradiation resistant – there was an essentially unchanged UPF property before and after UV (370 nm) 40 h irradiation, within experimental error. Without the surface modification contributions of the ZnO additive specifically, the UPF values were unremarkable and indistinguishable from the uncoated reference substrate.

Impermanence to washing is frequently encountered for fabric coatings. However, silica has often been reported as an effective method for stabilizing nanomaterials on textiles.[107] Empirically, UPF, water contact angle and sliding angle data were reacquired for all samples after three accelerated wash cycles of laundering (*i.e.*, equivalent to nine standard domestic wash cycles). While performance deteriorations were seen in all conditions, the performance retention in coated fabrics as compared to the cotton reference standard showed that at least some coating material remained adhered to the substrate. Thus, despite some loss of coating material, there is a degree of persistence in the silica-ZnO NP functional performance, such that the substrate could still be reused for water-repellency and/or UV-protective functions. It should be noted that treatment of any kind will have a deleterious effect on pristine cotton fabric, and this explains the discrepancy in values between the pristine substrates, and the chemically-treated, coated variants, even without the laundering steps.

4. Conclusions

This work provides sustainable routes to functionally-coated fabrics with UV-shielding capability and stable, high hydrophobicity (up to 148°), while still retaining excellent water vapor permeability properties. Woven cotton substrates were alternatively dip-coated with either silica or silica-ZnO NP. The resultant coatings were sparsely distributed throughout the entire fibrous surface. The choice of binder/hydrophobizing agent was important in decreasing the surface energy, increasing surface roughening and NP-retention; a higher relative OTES binder concentration allowed for greater additive loading onto the substrate.

These NP intermediate coating layers provide otherwise rough, porous fabric substrates with stable and reliably high hydrophobic properties with low sliding angles. Fabrics imparted with silica-ZnO NP UV-absorbers exhibited markedly superior UV shielding properties with UPF values far in excess of 50, albeit with a slight decrease in relative hydrophobic character as compared to the solely silica-based coatings. Such combined UPF and water contact angle properties were stable even after 40 h continuous exposure to UV-radiation, avoiding the otherwise commonly encountered UV-induced hydrophobic-to-hydrophilic transition for ZnO. These properties also showed persistence, albeit with an associated performance decline, after being subjected to accelerated laundering treatments. Thicker coatings and/or more resilient binders could perhaps overcome this issue, for longer-lasting performance retention.

Durably hydrophobic and UV protective textiles have potential applications in outdoor garments and architectural fabrics, which could help defend against extreme weather environments, protecting the wearer during open-air activities. However, an ideal treatment for scalability would involve water-processable polymers and methods, and so further procedural refinement in this direction would be valuable. In addition, further study is necessary to characterize the mechanisms contributing to these hydrophobic surfaces. Such work is underway.

Consent for publication

All authors agree to the submission and publication of article materials.

Author contributions

All authors contributed meaningfully to all aspects of experimentation, analysis and composition.

Conflicts of interest

There are no known conflicts to declare.

Acknowledgements

References

1 J. Ma, L. E. Porath, M. F. Haque, S. Sett, K. F. Rabbi, S. Nam, N. Miljkovic and C. M. Evans, Ultra-thin self-healing vitrimer coatings for durable hydrophobicity, *Nat. Commun.*, 2021, **12**(1), 5210, DOI: **10.1038/s41467-021-25508-4**.

2 Z. Li, J. Wu, Y. Wang, Y. Li, G. Huang, B. Fei, Z. Xu, Y. Zhang and Y. Li, A facile approach to obtain super-hydrophobicity for cotton fiber fabrics, *RSC Adv.*, 2023, **13**(14), 9237–9241, DOI: **10.1039/D2RA08189J**.

3 J. Qian, Q. Dong, K. Chun, D. Zhu, X. Zhang, Y. Mao, J. N. Culver, S. Tai, J. R. German, D. P. Dean, J. T. Miller, L. Wang, T. Wu, T. Li, A. H. Brozena, R. M. Briber, D. K. Milton, W. E. Bentley and L. Hu, Highly stable, antiviral, antibacterial cotton textiles *via* molecular engineering, *Nat. Nanotechnol.*, 2023, **18**(2), 168–176, DOI: **10.1038/s41565-022-01278-y**.

4 R. Yu, M. Tian, L. Qu, S. Zhu, J. Ran and R. Liu, Fast and simple fabrication of SiO$_2$/poly(vinylidene fluoride) coated cotton fabrics with asymmetric wettability *via* a facile spray-coating route, *Text. Res. J.*, 2019, **89**(6), 1013–1026, DOI: **10.1177/0040517518760755**.

5 C. Hou and C. Cao, Superhydrophobic cotton fabric membrane prepared by fluoropolymers and modified nano-SiO$_2$ used for oil/water separation, *RSC Adv.*, 2021, **11**(50), 31675–31687, DOI: **10.1039/D1RA06393F**.

6 J. Zhao, W. Zhu, X. Wang, L. Liu, J. Yu and B. Ding, Fluorine-free waterborne coating for environmentally friendly, robustly water-resistant, and highly breathable fibrous textiles, *ACS Nano*, 2020, **14**(1), 1045–1054, DOI: **10.1021/acsnano.9b08595**.

7 H. Peng, Synthesis and application of fluorine-containing polymers with low surface energy, *Polym. Rev.*, 2019, **59**(4), 739–757, DOI: **10.1080/15583724.2019.1636390**.

8 Y. Itoh, S. Chen, R. Hirahara, T. Konda, T. Aoki, T. Ueda, I. Shimada, J. J. Cannon, C. Shao, J. Shiomi, K. V. Tabata, H. Noji, K. Sato and T. Aida, Ultrafast water permeation

through nanochannels with a densely fluorous interior surface, *Science*, 2022, **376**(6594), 738–743, DOI: **10.1126/science.abd0966**.

9 M. Dai, Y. Zhai and Y. Zhang, A green approach to preparing hydrophobic, electrically conductive textiles based on waterborne polyurethane for electromagnetic interference shielding with low reflectivity, *Chem. Eng. J.*, 2021, **421**, 127749, DOI: **10.1016/j.cej.2020.127749**.

10 J.-M. Jian, Y. Guo, L. Zeng, L. Liang-Ying, X. Lu, F. Wang and E. Y. Zeng, Global distribution of perfluorochemicals (PFCs) in potential human exposure source–a review, *Environ. Int.*, 2017, **108**, 51–62, DOI: **10.1016/j.envint.2017.07.024**.

11 H. Ye, L. Zhu, W. Li, H. Liu and H. Chen, Constructing fluorine-free and cost-effective superhydrophobic surface with normal-alcohol-modified hydrophobic SiO$_2$ nanoparticles, *ACS Appl. Mater. Interfaces*, 2017, **9**(1), 858–867, DOI: **10.1021/acsami.6b12820**.

12 S. Liu, W. Wan, X. Zhang, A. De Crema and S. Seeger, All-organic fluorine-free superhydrophobic bulk material with mechanochemical robustness and photocatalytic functionality, *Chem. Eng. J.*, 2020, **385**, 123969, DOI: **10.1016/j.cej.2019.123969**.

13 S. Moradi, P. Englezos and S. G. Hatzikiriakos, Contact angle hysteresis: surface morphology effects, *Colloid Polym. Sci.*, 2013, **291**(2), 317–328, DOI: **10.1007/s00396-012-2746-3**.

14 Z. Shi, I. Wyman, G. Liu, H. Hu, H. Zou and J. Hu, Preparation of water-repellent cotton fabrics from fluorinated diblock copolymers and evaluation of their durability, *Polymer*, 2013, **54**(23), 6406–6414, DOI: **10.1016/j.polymer.2013.09.043**.

15 S. Park, J. Kim and C. H. Park, Superhydrophobic textiles: review of theoretical definitions, fabrication and functional evaluation, *J. Eng. Fiber. Fabr.*, 2015, **10**(4), 155892501501000, DOI: **10.1177/155892501501000401**.

16 H. Teisala, M. Tuominen and J. Kuusipalo, Superhydrophobic coatings on cellulose-based materials: fabrication, properties, and applications, *Adv. Mater. Interfaces*, 2014, **1**(1), 1300026, DOI: **10.1002/admi.201300026**.

17 N. Gao, F. Geyer, D. W. Pilat, S. Wooh, D. Vollmer, H.-J. Butt and R. Berger, How drops start sliding over solid surfaces, *Nat. Phys.*, 2018, **14**(2), 191–196, DOI: **10.1038/nphys4305**.

18 X. Li, P. Bista, A. Z. Stetten, H. Bonart, M. T. Schür, S. Hardt, F. Bodziony, H. Marschall, A. Saal, X. Deng, R. Berger, S. A. L. Weber and H.-J. Butt, Spontaneous charging affects the motion of sliding drops, *Nat. Phys.*, 2022, **18**, 713–719, DOI: **10.1038/s41567-022-01563-6**.

19 M. Zahid, J. A. Heredia-Guerrero, A. Athanassiou and I. S. Bayer, Robust water repellent treatment for woven cotton fabrics with eco-friendly polymers, *Chem. Eng. J.*, 2017, **319**, 321–332, DOI: **10.1016/j.cej.2017.03.006**.

20 H. P. Ming, C. Y. Chan, S. Mutalik, M. W. Younas, A. Pragya and N. Noor, Sonochemical routes to superhydrophobic soft matter coatings: comparing silica and copper oxide

coatings on polyester fabric, *Ind. Eng. Chem. Res.*, 2022, **61**(51), 18729–18743, DOI: **10.1021/acs.iecr.2c02939**.

21 X. Hu, Y. Zhang, J. Zhang, H. Yang, F. Wang, B. Fei and N. Noor, Sonochemically-coated transparent wood with ZnO: passive radiative cooling materials for energy saving applications, *Renewable Energy*, 2022, **193**, 398–406, DOI: **10.1016/j.renene.2022.05.008**.

22 M. S. Selim, M. A. Shenashen, A. Elmarakbi, N. A. Fatthallah, S. Hasegawa and S. A. El- Safty, Synthesis of ultrahydrophobic and thermally stable inorganic–organic nanocomposites for self-cleaning foul release coatings, *Chem. Eng. J.*, 2017, **320**, 653–666, DOI: **10.1016/j.cej.2017.03.067**.

23 N. Noor, S. Mutalik, M. W. Younas, A. Pragya, X. Hu, C. Y. Ho, K. M. Yu and B. Fei, Sonochemical coating of textiles with zinc oxide: robust, silver-seeded growth on cotton for effective UV shielding, *ACS Appl. Eng. Mater.*, 2023, **1**(12), 3254–3267, DOI: **10.1021/acsaenm.3c00578**.

24 R. Huang, S. Zhang, W. Zhang and X. Yang, Progress of zinc oxide-based nanocomposites in the textile industry, *IET Collab. Intell. Manuf.*, 2021, **3**(3), 281–289, DOI: **10.1049/cim2.12029**.

25 K.-B. Kim, Y. J. Y. W. Kim, S. K. Lim, T. H. Roh, D. Y. Bang, S. M. Choi, D. S. Lim, Y. J. Y. W. Kim, S.-H. Baek, M.-H. M.-K. Kim, H.-S. Seo, M.-H. M.-K. Kim, H. S. Kim, J. Y. Lee, S. Kacew and B.-M. Lee, Risk assessment of zinc oxide, a cosmetic ingredient used as a UV filter of sunscreens, *J. Toxicol. Environ. Health, Part B*, 2017, **20**(3), 155–182, DOI: **10.1080/10937404.2017.1290516**.

26 R. Kumar, G. Deep and R. Agarwal, An overview of ultraviolet b radiation-induced skin cancer chemoprevention by silibinin, *Curr. Pharmacol. Rep.*, 2015, **1**(3), 206–215, DOI: **10.1007/s40495-015-0027-9**.

27 R. M. Lucas, R. E. Neale, S. Madronich and R. L. McKenzie, Are current guidelines for sun protection optimal for health? Exploring the evidence, *Photochem. Photobiol. Sci.*, 2018, **17**(12), 1956–1963, DOI: **10.1039/C7PP00374A**.

28 M. A. Grimes, The Effect of Sunlight and Other Factors on the Strength and Color of Cotton Fabrics, *J. Am. Med. Assoc.*, 1933, **101**(7), 550, DOI: **10.1001/jama.1933.02740320060037**.

29 M. Zhang, B. Tang, L. Sun and X. Wang, Reducing photoyellowing of wool fabrics with silica coated ZnO nanoparticles, *Text. Res. J.*, 2014, **84**(17), 1840–1848, DOI: **10.1177/0040517514530028**.

30 C. Jiang, W. Liu, M. Yang, C. Liu, S. He, Y. Xie and Z. Wang, Robust multifunctional superhydrophobic fabric with UV Induced reversible wettability, photocatalytic self-cleaning property, and oil-water separation *via* thiol-ene click chemistry, *Appl. Surf. Sci.*, 2019, **463**, 34–44, DOI: **10.1016/j.apsusc.2018.08.197**.

31 G. R. Chagas and D. E. Weibel, UV-Induced switchable wettability between superhydrophobic and superhydrophilic polypropylene surfaces with an improvement of adhesion properties, *Polym. Bull.*, 2017, **74**(6), 1965–1978, DOI: **10.1007/s00289-016-1817-x**.

32 A. P. S. Prasanna, K. S. Venkataprasanna, B. Pannerselvam, V. Asokan, R. S. Jeniffer and G. D. Venkatasubbu, Multifunctional ZnO/SiO$_2$ core/shell nanoparticles for bioimaging and drug delivery application, *J. Fluoresc.*, 2020, **30**(5), 1075–1083, DOI: **10.1007/s10895-020-02578-z**.

33 M. E. El-Naggar, A. G. Hassabo, A. L. Mohamed and T. I. Shaheen, Surface modification of SiO$_2$ coated ZnO Nanoparticles for multifunctional cotton fabrics, *J. Colloid Interface Sci.*, 2017, **498**, 413–422, DOI: **10.1016/j.jcis.2017.03.080**.

34 H. Barani, Preparation of antibacterial coating based on *in situ* synthesis of ZnO/SiO$_2$ hybrid nanocomposite on cotton fabric, *Appl. Surf. Sci.*, 2014, **320**, 429–434, DOI: **10.1016/j.apsusc.2014.09.102**.

35 S. L. Chia and D. T. Leong, Reducing ZnO nanoparticles toxicity through silica coating, *Heliyon*, 2016, **2**(10), e00177, DOI: **10.1016/j.heliyon.2016.e00177**.

36 F. Lambiase and F. Liu, Recent advances in metal-polymer joining processes, in *Joining Processes for Dissimilar and Advanced Materials*, Elsevier, 2022, pp. 123–151, DOI: **10.1016/B978-0-323-85399-6.00007-2**.

37 Y. Xie, C. A. S. Hill, Z. Xiao, H. Militz and C. Mai, Silane coupling agents used for natural fiber/polymer composites: a review, *Composites Part A*, 2010, **41**(7), 806–819, DOI: **10.1016/j.compositesa.2010.03.005**.

38 M. Agostini, G. Greco and M. Cecchini, Polydimethylsiloxane (PDMS) irreversible bonding to untreated plastics and metals for microfluidics applications, *APL Mater.*, 2019, **7**(8), 081108, DOI: **10.1063/1.5070136**.

39 M. V. Hoang, H.-J. Chung and A. L. Elias, Irreversible Bonding of polyimide and polydimethylsiloxane (PDMS) based on a thiol-epoxy click Reaction, *J. Micromech. Microeng.*, 2016, **26**(10), 105019, DOI: **10.1088/0960-1317/26/10/105019**.

40 B. N. Sahoo, S. Nanda, J. A. Kozinski and S. K. Mitra, PDMS/Camphor soot composite coating: towards a self-healing and a self-cleaning superhydrophobic surface, *RSC Adv.*, 2017, **7**(25), 15027–15040, DOI: **10.1039/C6RA28581C**.

41 S. Xiao, P. Xu, Q. Peng, J. Chen, J. Huang, F. Wang and N. Noor, Layer-by-layer assembly of polyelectrolyte multilayer onto PET fabric for highly tunable dyeing with water soluble dyestuffs, *Polymers*, 2017, **9**(12), 735, DOI: **10.3390/polym9120735**.

42 Y. Feng, Z. Xu, C. Peng, H. Huang and J. Hu, A facile route to obtain binary micro-nano roughness on composite coating surface, *Eur. Phys. J. Appl. Phys.*, 2018, **82**(2), 21302, DOI: **10.1051/epjap/2018170209**.

43 S. Arya, P. Mahajan, S. Mahajan, A. Khosla, R. Datt, V. Gupta, S.-J. Young and S. K. Oruganti, Review—Influence of processing parameters to control morphology and optical properties of sol–gel synthesized ZnO nanoparticles, *ECS J. Solid State Sci. Technol.*, 2021, **10**(2), 023002, DOI: **10.1149/2162-8777/abe095**.

44 P. P. Ghimire and M. Jaroniec, Renaissance of stöber method for synthesis of colloidal particles: new developments and opportunities, *J. Colloid Interface Sci.*, 2021, **584**, 838–865, DOI: **10.1016/j.jcis.2020.10.014**.

45 W. Stöber, A. Fink and E. Bohn, Controlled growth of monodisperse silica spheres in the micron size range, *J. Colloid Interface Sci.*, 1968, **26**(1), 62–69, DOI: **10.1016/0021-9797(68)90272-5**.

46 H. N. Azlina, J. N. Hasnidawani, H. Norita and S. N. Surip, Synthesis of SiO$_2$ nanostructures using sol–gel method, *Acta Phys. Pol., A*, 2016, **129**(4), 842–844, DOI: **10.12693/APhysPolA.129.842**.

47 H.-L. Xia and F.-Q. Tang, Surface synthesis of zinc oxide nanoparticles on silica spheres: preparation and characterization, *J. Phys. Chem. B*, 2003, **107**(35), 9175–9178, DOI: **10.1021/jp0261511**.

48 J. Zhai, X. Tao, Y. Pu, X.-F. Zeng and J.-F. Chen, Core/shell structured ZnO/SiO$_2$ nanoparticles: preparation, characterization and photocatalytic property, *Appl. Surf. Sci.*, 2010, **257**(2), 393–397, DOI: **10.1016/j.apsusc.2010.06.091**.

49 A. Pragya, S. Mutalik, M. W. Younas, S.-K. Pang, P.-K. So, F. Wang, Z. Zheng and N. Noor, Dynamic Cross-linking of an alginate–acrylamide tough hydrogel system: time-resolved *in situ* mapping of gel self-assembly, *RSC Adv.*, 2021, **11**(18), 10710–10726, DOI: **10.1039/D0RA09210J**.

50 S. Pajevic, R. Bansil, C. Konak, S. Pajevič, R. Bansil, Č. Koňák, S. Pajevic, R. Bansil and C. Konak, Dynamic light scattering study of linear polyelectrolyte diffusion in gels, *Macromolecules*, 1995, **28**(22), 7536–7542, DOI: **10.1021/ma00126a035**.

51 Y. Yuan and T. R. Lee, Contact angle and wetting properties, in *Surface Science Techniques*, ed. G. Bracco, and B. Holst, Springer, Berlin, Heidelberg, 2013, pp. 3–34, DOI: **10.1007/978-3-642-34243-1_1**.

52 C. E. Cansoy, The effect of drop size on contact angle measurements of superhydrophobic surfaces, *RSC Adv.*, 2014, **4**(3), 1197–1203, DOI: **10.1039/C3RA45947K**.

53 H.-A. Kim, Moisture vapor resistance of coated and laminated breathable fabrics using evaporative wet heat transfer method, *Coatings*, 2021, **11**(10), 1157, DOI: **10.3390/coatings11101157**.

54 Q. Chen, D. Shou, B. Fu, R. Zheng and J. Fan, Development of moisture management knitted fabrics integarated with non-smooth concave surface and mesh structure, *Fibers Polym.*, 2022, **23**(4), 1142–1149, DOI: **10.1007/s12221-022-4420-9**.

55 W. Wong, J. K.-C. Lam, C. Kan and R. Postle, Influence of knitted fabric construction on the ultraviolet protection factor of greige and bleached cotton fabrics, *Text. Res. J.*, 2013, **83**(7), 683–699, DOI: **10.1177/0040517512467078**.

56 C. Kan, L. Yam and S. Ng, Effect of stretching on ultraviolet protection of cotton and cotton/coolmax blended weft knitted fabric in a wet state, *Materials*, 2013, **7**(1), 58–74, DOI: **10.3390/ma7010058**.

57 Y. Xu, D. Wu, Y. Sun, H. Gao, H. Yuan and F. Deng, A New study on the kinetics of stöber synthesis by *in situ* liquid 29Si NMR, *J. Sol-Gel Sci. Technol.*, 2007, **42**(1), 13–20, DOI: **10.1007/s10971-006-1518-2**.

58 Z. A. Alothman, Review: fundamental aspects of silicate mesoporous materials, *Materials*, 2012, **5**(12), 2874–2902, DOI: **10.3390/ma5122874**.

59 L. T. Zhuravlev and V. V. Potapov, Density of silanol groups on the surface of silica precipitated from a hydrothermal solution, *Russ. J. Phys. Chem.*, 2006, **80**(7), 1119–1128, DOI: **10.1134/S0036024406070211**.

60 H. Kaur, S. Chaudhary, H. Kaur, M. Chaudhary and K. C. Jena, Hydrolysis and condensation of tetraethyl orthosilicate at the air–aqueous interface: implications for silica nanoparticle formation, *ACS Appl. Nano Mater.*, 2022, **5**(1), 411–422, DOI: **10.1021/acsanm.1c03250**.

61 J. Wei, M. S. Saharudin, T. Vo and F. Inam, Effects of surfactants on the properties of epoxy/graphene nanocomposites, *J. Reinf. Plast. Compos.*, 2018, **37**(14), 960–967, DOI: **10.1177/0731684418765369**.

62 X. Yan, L. Chai, Q. Li, L. Ye, B. Yang and Q. Wang, Pathway of zinc oxide formation by seed-assisted and controlled double-jet precipitation, *CrystEngComm*, 2016, **18**(6), 924–929, DOI: **10.1039/C5CE01916H**.

63 R. Somoghi, V. Purcar, E. Alexandrescu, I. C. Gifu, C. M. Ninciuleanu, C. M. Cotrut, F. Oancea and H. Stroescu, Synthesis of zinc oxide nanomaterials *via* sol–gel process with anti-corrosive effect for Cu, Al and Zn metallic substrates, *Coatings*, 2021, **11**(4), 444, DOI: **10.3390/coatings11040444**.

64 M. Zare, K. Namratha, K. Byrappa, D. M. Surendra, S. Yallappa and B. Hungund, Surfactant assisted solvothermal synthesis of ZnO nanoparticles and study of their antimicrobial and antioxidant properties, *J. Mater. Sci. Technol.*, 2018, **34**(6), 1035–1043, DOI: **10.1016/j.jmst.2017.09.014**.

65 F. Rizzi, R. Castaldo, T. Latronico, P. Lasala, G. Gentile, M. Lavorgna, M. Striccoli, A. Agostiano, R. Comparelli, N. Depalo, M. L. Curri and E. Fanizza, High surface area mesoporous silica nanoparticles with tunable size in the sub-micrometer regime: insights on the size and porosity control mechanisms, *Molecules*, 2021, **26**(14), 4247, DOI: **10.3390/molecules26144247**.

66 G. Vijayaprasath, R. Murugan, Y. Hayakawa and G. Ravi, Optical and magnetic studies on Gd doped ZnO nanoparticles synthesized by co-precipitation method, *J. Lumin.*, 2016, **178**, 375–383, DOI: **10.1016/j.jlumin.2016.06.004**.

67 A. A. Barzinjy and H. H. Azeez, Green synthesis and characterization of zinc oxide nanoparticles using eucalyptus globulus labill. Leaf extract and zinc nitrate hexahydrate salt, *SN Appl. Sci.*, 2020, **2**(5), 991, DOI: **10.1007/s42452-020-2813-1**.

68 H. M. H. Al-Kordy, S. A. Sabry and M. E. M. Mabrouk, Statistical optimization of experimental parameters for extracellular synthesis of zinc oxide nanoparticles by a novel haloalaliphilic *Alkalibacillus* Sp.W7, *Sci. Rep.*, 2021, **11**(1), 10924, DOI: **10.1038/s41598-021-90408-y**.

69 S. Ghose and D. Jana, Defect dependent inverted shift of band structure for ZnO nanoparticles, *Mater. Res. Express*, 2019, **6**(10), 105907, DOI: **10.1088/2053-1591/ab3b15**.

70 A. Furube and S. Hashimoto, Insight into plasmonic hot-electron transfer and plasmon molecular drive: new dimensions in energy conversion and nanofabrication, *NPG Asia Mater.*, 2017, **9**(12), e454, DOI: **10.1038/am.2017.191**.

71 M. H. J. H. Al-Atia, H. K. Saeed, A. R. Fliayh and A. J. Addie, Investigating the effects of calcination temperatures on the structure of modified nanosilica prepared by sol–gel, *Colloids Surf., A*, 2017, **520**, 590–596, DOI: **10.1016/j.colsurfa.2017.02.020**.

72 D. Guo, K. Sato, S. Hibino, T. Takeuchi, H. Bessho and K. Kato, Low-temperature preparation of (002)-oriented zno thin films by sol–gel method, *Thin Solid Films*, 2014, **550**, 250–258, DOI: **10.1016/j.tsf.2013.11.004**.

73 S. Bhattacharjee, DLS and zeta potential – what they are and what they are not?, *J. Controlled Release*, 2016, **235**, 337–351, DOI: **10.1016/j.jconrel.2016.06.017**.

74 R. Singh and R. Bhateria, Core–shell nanostructures: a simplest two-component system with enhanced properties and multiple applications, *Environ. Geochem. Health*, 2021, **43**(7), 2459–2482, DOI: **10.1007/s10653-020-00766-1**.

75 M. B. Gawande, A. Goswami, T. Asefa, H. Guo, A. V. Biradar, D.-L. Peng, R. Zboril and R. S. Varma, Core–shell nanoparticles: synthesis and applications in catalysis and electrocatalysis, *Chem. Soc. Rev.*, 2015, **44**(21), 7540–7590, DOI: **10.1039/C5CS00343A**.

76 S. Rades, V.-D. Hodoroaba, T. Salge, T. Wirth, M. P. Lobera, R. H. Labrador, K. Natte, T. Behnke, T. Gross and W. E. S. Unger, High-resolution imaging with SEM/T-SEM, EDX and SAM as a combined methodical approach for morphological and elemental analyses of single engineered nanoparticles, *RSC Adv.*, 2014, **4**(91), 49577–49587, DOI: **10.1039/C4RA05092D**.

77 S. Thakur and S. K. Mandal, Precursor- and time-dependent morphological evolution of ZnO nanostructures for comparative photocatalytic activity and adsorption dynamics with methylene blue dye, *ACS Omega*, 2020, **5**(27), 16670–16680, DOI: **10.1021/acsomega.0c01555**.

78 Y. Pu, Y. Niu, Y. Wang, S. Liu and B. Zhang, Statistical morphological identification of low-dimensional nanomaterials by using TEM, *Particuology*, 2022, **61**, 11–17, DOI: **10.1016/j.partic.2021.03.013**.

79 A. Bai, H. Song, G. He, Q. Li, C. Yang, L. Tang and Y. Yu, Facile synthesis of core–shell structured ZrO$_2$@SiO$_2$ *via* a modified stöber method, *Ceram. Int.*, 2016, **42**(6), 7583–7592, DOI: **10.1016/j.ceramint.2016.01.166**.

80 P.-H. Shih and S. Wu, Growth mechanism studies of ZnO nanowires: experimental observations and short-circuit diffusion analysis, *Nanomaterials*, 2017, **7**(7), 188, DOI: **10.3390/nano7070188**.

81 H. Bai, L. Wang, J. Ju, R. Sun, Y. Zheng and L. Jiang, Efficient water collection on integrative bioinspired surfaces with star-shaped wettability patterns, *Adv. Mater.*, 2014, **26**(29), 5025–5030, DOI: **10.1002/adma.201400262**.

82 Y. Zhao, Z. Xu, X. Wang and T. Lin, Photoreactive azido-containing silica nanoparticle/polycation multilayers: durable superhydrophobic coating on cotton fabrics, *Langmuir*, 2012, **28**(15), 6328–6335, DOI: **10.1021/la300281q**.

83 X. Dong, A. Gusev and D. M. Hercules, Characterization of polysiloxanes with different functional groups by time-of-flight secondary ion mass spectrometry, *J. Am. Soc. Mass Spectrom.*, 1998, **9**(4), 292–298, DOI: **10.1016/S1044-0305(98)00003-8**.

84 Y.-T. Tsai, I. V. Maggay, A. Venault and Y.-F. Lin, Fluorine-free and hydrophobic/oleophilic PMMA/PDMS electrospun nanofibrous membranes for gravity-driven removal of water from oil-rich emulsions, *Sep. Purif. Technol.*, 2021, **279**, 119720, DOI: **10.1016/j.seppur.2021.119720**.

85 I. Sulym, O. Goncharuk, D. Sternik, K. Terpilowski, A. Derylo-Marczewska, M. V. Borysenko and V. M. Gun'ko, Nanooxide/polymer composites with silica@PDMS and ceria–zirconia–silica@PDMS: textural, morphological, and hydrophilic/hydrophobic features, *Nanoscale Res. Lett.*, 2017, **12**(1), 152, DOI: **10.1186/s11671-017-1935-x**.

86 T. Wang, Z. Lu, X. Wang, Z. Zhang, Q. Zhang, B. Yan and Y. Wang, A compound of ZnO/PDMS with photocatalytic, self-cleaning and antibacterial properties prepared *via* two-step method, *Appl. Surf. Sci.*, 2021, **550**, 149286, DOI: **10.1016/j.apsusc.2021.149286**.

87 K. Jeronimo, V. Koutsos, R. Cheung and E. Mastropaolo, PDMS-ZnO piezoelectric nanocomposites for pressure sensors, *Sensors*, 2021, **21**(17), 5873, DOI: **10.3390/s21175873**.

88 L. Shen, Y. Pan and H. Fu, Fabrication of UV curable coating for super hydrophobic cotton fabrics, *Polym. Eng. Sci.*, 2019, **59**(s2), E452–E459, DOI: **10.1002/pen.25082**.

89 S. Gorgutsa, K. Bachus, S. LaRochelle, R. D. Oleschuk and Y. Messaddeq, Washable hydrophobic smart textiles and multi-material fibers for wireless communication, *Smart Mater. Struct.*, 2016, **25**(11), 115027, DOI: **10.1088/0964-1726/25/11/115027**.

90 K.-M. Li, J.-G. Jiang, S.-C. Tian, X.-J. Chen and F. Yan, Influence of Silica types on synthesis and performance of amine–silica hybrid materials used for CO_2 capture, *J. Phys. Chem. C*, 2014, **118**(5), 2454–2462, DOI: **10.1021/jp408354r**.

91 T. Pipatchanchai and K. Srikulkit, Hydrophobicity Modification of woven cotton fabric by hydrophobic fumed silica coating, *J. Sol-Gel Sci. Technol.*, 2007, **44**(2), 119–123, DOI: **10.1007/s10971-007-1609-8**.

92 F. Ebrahimi, R. Farazi, E. Z. Karimi and H. Beygi, Dichlorodimethylsilane mediated one-step synthesis of hydrophilic and hydrophobic silica nanoparticles, *Adv. Powder Technol.*, 2017, **28**(3), 932–937, DOI: **10.1016/j.apt.2016.12.022**.

93 M. H. Shim, J. Kim and C. H. Park, The effects of surface energy and roughness on the hydrophobicity of woven fabrics, *Text. Res. J.*, 2014, **84**(12), 1268–1278, DOI: **10.1177/0040517513495945**.

94 K. Jeyasubramanian, G. S. Hikku, A. V. M. Preethi, V. S. Benitha and N. Selvakumar, Fabrication of water repellent cotton fabric by coating nano particle impregnated hydrophobic additives and its characterization, *J. Ind. Eng. Chem.*, 2016, **37**, 180–189, DOI: **10.1016/j.jiec.2016.03.023**.

95 P. Mukerjee, The nature of the association equilibria and hydrophobic bonding in aqueous solutions of association colloids, *Adv. Colloid Interface Sci.*, 1967, **1**(3), 242–275, DOI: **10.1016/0001-8686(67)80005-8**.

96 A. B. D. Cassie and S. Baxter, Wettability of porous surfaces, *Trans. Faraday Soc.*, 1944, **40**, 546, DOI: **10.1039/tf9444000546**.

97 M. Beitollahpoor, M. Farzam and N. S. Pesika, Determination of the sliding angle of water drops on surfaces from friction force measurements, *Langmuir*, 2022, **38**(6), 2132–2136, DOI: **10.1021/acs.langmuir.1c03206**.

98 D. Liu, A. M. Pourrahimi, L. K. H. Pallon, R. L. Andersson, M. S. Hedenqvist, U. W. Gedde and R. T. Olsson, Morphology and properties of silica-based coatings with different functionalities for Fe_3O_4, ZnO and Al_2O_3 nanoparticles, *RSC Adv.*, 2015, **5**(59), 48094–48103, DOI: **10.1039/C5RA04452A**.

99 M. T. Z. Myint, N. S. Kumar, G. L. Hornyak and J. Dutta, Hydrophobic/hydrophilic switching on zinc oxide micro-textured surface, *Appl. Surf. Sci.*, 2013, **264**, 344–348, DOI: **10.1016/j.apsusc.2012.10.024**.

100 C.-H. Xue, W. Yin, P. Zhang, J. Zhang, P.-T. Ji and S.-T. Jia, UV-durable superhydrophobic textiles with UV-shielding properties by introduction of ZnO/SiO_2 core/shell nanorods on PET fibers and hydrophobization, *Colloids Surf., A*, 2013, **427**, 7–12, DOI: **10.1016/j.colsurfa.2013.03.021**.

101 J. Lv, Z. Zhou, F. Wang, C. Liu, W. Gong, X. Chen, G. He, S. Shi, X. Song, Z. Sun and Y. Tang, The improved photo-induced hydrophilicity of ZnO by adjusting the solution concentration, *Phys. Scr.*, 2013, **88**(4), 045602, DOI: **10.1088/0031-8949/88/04/045602**.

102 J. Holländer, R. Hakala, J. Suominen, N. Moritz, J. Yliruusi and N. Sandler, 3D printed UV light cured polydimethylsiloxane devices for drug delivery, *Int. J. Pharm.*, 2018, **544**(2), 433–442, DOI: **10.1016/j.ijpharm.2017.11.016**.

103 A. N. D. Krupa and R. Vimala, Evaluation of tetraethoxysilane (TEOS) sol–gel coatings, modified with green synthesized zinc oxide nanoparticles for combating microfouling, *Mater. Sci. Eng., C*, 2016, **61**, 728–735, DOI: **10.1016/j.msec.2016.01.013**.

104 S. Lee and S. K. Obendorf, Barrier effectiveness and thermal comfort of protective clothing materials, *J. Text. Inst.*, 2007, **98**(2), 87–98, DOI: **10.1533/joti.2005.0143**.

105 L. Wang, X. Zhang, Y. Fu, B. Li and Y. Liu, Bioinspired preparation of ultrathin SiO_2 shell on ZnO nanowire array for ultraviolet-durable superhydrophobicity, *Langmuir*, 2009, **25**(23), 13619–13624, DOI: **10.1021/la901998p**.

106 S. Riaz, M. Ashraf, T. Hussain, M. T. Hussain, A. Younus, M. Raza and A. Nosheen, Selection and optimization of silane coupling agents to develop durable functional cotton fabrics using TiO$_2$ nanoparticles, *Fibers Polym.*, 2021, **22**(1), 109–122, DOI: **10.1007/s12221-021-9245-4**.

107 M. P. Gashti, M. Y. Navid and M. H. Rahimi, Coating of macroemulsion and microemulsion silicones on poly(ethylene terephthalate) fibers: evaluation of the thermal properties and flammability, *J. Appl. Polym. Sci.*, 2012, **125**(2), 1430–1438, DOI: **10.1002/app.35601**.